https://doi.org/10.1016/j.nanoen.2021.106807

Fabric-Rebound Triboelectric Nanogenerators with Loops and Layered Structures for Energy Harvesting and Intelligent Wireless Monitoring of Human Motions

Chenghanzhi Jiang†, Cheuk Lam Lai†, Bingang Xu*, Mei Yi So, Zihua Li

Nanotechnology Center, Institute of Textiles and Clothing, The Hong Kong Polytechnic University, Hung Hom, Kowloon, Hong Kong, China.
† Authors contributed equally
* Corresponding author. Email: tcxubg@polyu.edu.hk

Abstract

Self-powered electronic textiles (e-textiles) and triboelectric nanogenerators (TENGs) have been explored for the development of energy-harvesting facilities which provide sustainable power supplements for portable, wearable, and low-energy electronics. However, it requires the features of excellent structural stability and superior capability in sensing applications. In this study, we present and develop a new kind of fabric-rebound triboelectric nanogenerator (FR-TENG) that could be used for efficient energy harvesting and self-powered sensing. For improvement of electric performance, a systematic study has also been carried out to investigate various structural parameters for the property optimization of FR-TENGs. The as-made FR-TENG has shown stable electric performance in energy harvesting, cyclic washing capability, and mechanical durability. The full-textile structure of FR-TENG enhances its adaptability and rebound ability, and the open-circuit voltage, short circuit current and power density of the FR-TENG reach up to 418.09 V, 65.85 μA and 199.14 $\mu W \cdot cm^{-2}$, respectively. Furthermore, the FR-TENGs are used as smart carpets to build up a self-powered, wireless and intelligent system for monitoring human motions. This study proposes a new perspective for an all-textile TENGs and shows the advanced human-machine software interface in sensing applications.

Keywords:
Triboelectric Nanogenerator; Energy Harvesting; Textiles; Wireless Intelligent System; Self-Powered Sensors

1 Introduction

The industrial revolution has arisen behind the urgent demands of developing a self-powered system for wearable electronics in multidisciplinary fields, including the artificial intelligence (AI) [1-3], Internet of Things (IoT) [4, 5], smart system for healthcare [6], etc. Regarding the semiconductor industry and 5G information technology, the application software (app) [7, 8] has

been easily accessible and widely spread through personal mobiles and computers, which makes a self-powered and intelligent system for human motion monitoring become possible in helping the high-risk group and controlling the flow of people. In terms of self-powered systems, there are various types of nanogenerators commonly adopted to convert the biomechanical energy into electric power, based on the transducing mechanisms of piezoelectricity [9, 50-52], triboelectricity [10], electromagnetism [11], etc. While most of the self-powered sensing applications are relied on the ambient surroundings [12] or biological connections [13, 14], the triboelectric nanogenerator (TENG) [15, 53] shows its advantages in low cost, less dependence, high voltage output and good energy conversion efficiency.

According to the conversion mechanism of the TENG [10, 16], it can convert biomechanical energy into electric energy based on the coupled combination of triboelectrification and electrostatic induction [54, 55]. Since the invention of TENGs by Prof. ZL Wang, the TENG has been proved for efficient harvesting energy from mechanical triggering, particularly with the contact-separation mode in the vertical direction. In the contact-separate mode of TENG [17], the supporters or spacers should be built between the two triboelectric materials for the separation after their contacts are forced by external impact. The initially effective spacer was an elastic sponge in TENG [18] and there have been also several other types of configurations such as 'Z' shape [19], wave structure [20] and 3D printing flexible structure (composite resin parts) [21]. Then, the self-powered electronic textiles (e-textiles) were endowed with the abilities of energy harvesting by the integration of traditional textiles and functional fibre materials [22-25], which have been developed into all-textile energy harvesters [26-28], three-dimensional fabric structure [29], 3D braided structure [30], etc. These methods of self-powered systems can have realistic applications in energy storage [31, 32] for lighting/flickering LEDs [56-58], buzzing devices, and driving other low-energy electronics [59], with the supply of biomechanical energy from human motions [33, 60, 61]. However, the usage of spacers could infect the actual electric performance of a TENG, and at the same time, the TENG-based e-textiles was in the dilemma of low power output. Despite the improvements in the triboelectric performance of nanomaterials [34-36] and its nanostructures [37-39], the problem of low power densities, weak sensing abilities, and poor durability remains due to their high resistance. Therefore, a new type of TENG-based e-textiles is vital for developing a self-powered and intelligent system with high power output and stable self-sustainable ability.

Herein, specifically composed of loops and layered structures, a new kind of fabric-rebound triboelectric nanogenerator (FR-TENG) is proposed and optimized to convert biomechanical energy into electric power and expand its application in intelligent and wireless monitoring of human motion with BLE 4.0. As the dielectric and electric layers of FR-TENG are completely

fabricated by triboelectric materials, the FR-TENG with the distinguishing features of ultra-flexibility, structural integrity, cyclic washability, and excellent mechanical durability is achieved. The loop structures formed between the dielectric and electric layers create a natural stable contact-separation space to support the FR-TENG with good compression resilience, enhance its electric performance, and improve its sensing capability in applications. Under 3 Hz frequency and 600 N external force, the FR-TENG module ($5 \times 5 \times 1\ cm$, length × width × height) can achieve an open-circuit voltage, short-circuit current and its power density of 466.61 V, 12.61 μA and 107.94 $\mu W \cdot cm^{-2}$, which can be used to light up LEDs, charge commercial capacitors, and power low-energy electronics. For harvesting biomechanical energy (~1.5 Hz, 50 kg), it reaches outputs of voltage, current and power density of 418.09 V, 65.85 μA and 199.14 $\mu W \cdot cm^{-2}$, respectively. Moreover, an intelligent wireless carpet system for monitoring human motions, fall detection and controlling the flow of people is developed and demonstrated. The FR-TENG as an e-textile has good performance in power output and sensitivity that extended its broad prospects in portable power sources, wireless monitoring applications and multifunctional human-machine interfaces.

2 Results and Discussions

Design and fabrication of FR-TENGs. Based on previous research, the electric performance of triboelectric nanogenerators (TENGs) has been well studied and enhanced with their conductive and dielectric materials, as well as their contacting structures. In this fabrication of FR-TENG, we have used the commercial $Cu\&Ni$ fabric (CNF) [40] as conductive fabrics for the electrification layer and the material for the electrode, because of its excellent performance, industrial maturity and ease obtaining. In meantime, the dielectric layer is composed of polymer materials that are doped the PDMS (Polydimethylsiloxane) with $BaTiO_3$ (Barium Titanate) nanoparticles [34], owing to their good adaptability, stable inherent biocompatibility, high water resistance and dominant ability to gain electrons from positive materials. The fabric processes the coating method [22, 41] to improve the electrical conductivity of FR-TENG as well as mechanical flexibility, elasticity, and robustness. As it is illustrated in Fig. 1(a), several conductive fabrics are cut as strips for coating with polymer materials on one side and then on the other side, which made the origin conductive fabrics into conductive composites coated with polymer materials. The conductive composites are applied as FR-TENG base layers (Fig. 1(b)) and FR-TENG base loops (Fig. 1(c)), which are the components of FR-TENG in Fig. 1(d). The front view of FR-TENG is shown in Fig. 1(f). And the inner view inside the single FR-TENG base loop is shown in Fig. 1(e), which indicates that the output electric performances and the mechanical properties have relationships with the circles of the FR-TENG base loops and the layers of the FR-TENG base (Supplementary Fig. S1).

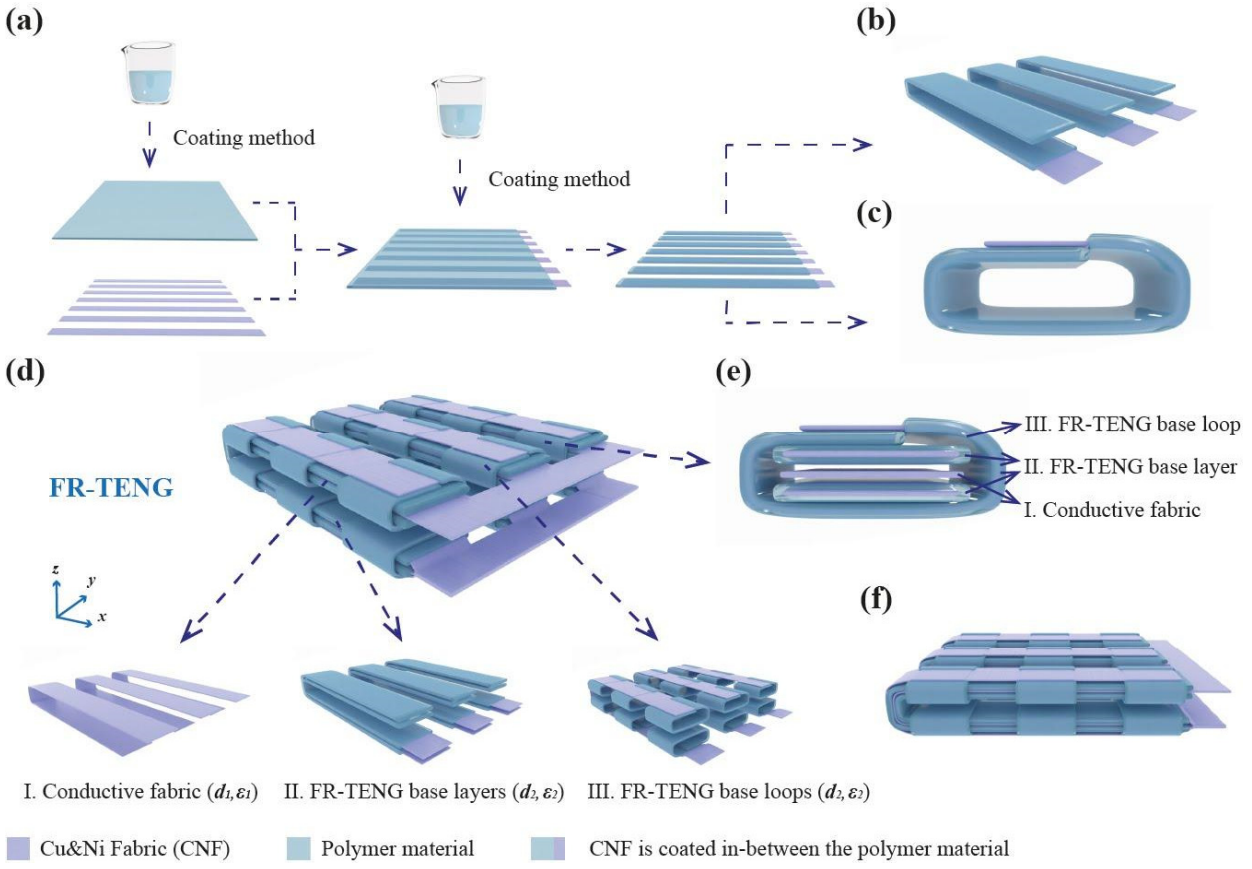

Fig. 1 Fabrication and structural diagram of the FR-TENG. (a) The schematic fabrication of FR-TENG in polymer material conducted CNF with coating method; (b) The sample of FR-TENG base layers; (c) The sample of FR-TENG base loops; (d) The view shows the structure of the FR-TENG and its parts: I. the conductive fabric cut as strips; II. FR-TENG base layers are the polymer material coated energy fabrics; III. FR-TENG base loops are the circle structures of the polymer material coated energy fabrics; (e) The demonstration of a single FR-TENG base loop with the conductive fabric and FR-TENG base layer; (f) The front view of the FR-TENG.

Operational mechanism. The physical mechanism of the FR-TENG is the combination of triboelectrification and electrostatic induction in the contact-mode TENG [17, 42], it creates triboelectric charges by distinct electrons of two different materials in the vertical direction (Fig. 2(b)). The cyclic contact-separation processes between the conductive fabrics, FR-TENG base layers and FR-TENG base loops are equivalent to the motions of compression and release (Fig. 2(c)). Considering the polymer materials have a dominant ability to gain electrons from conductive fabrics [34], the surface of polymer materials is apt to be negatively charged, while the outer conductive fabrics tend to be positively charged, in the relative contact and separation processes. When a pressing force is applied to the FR-TENG (Fig. 2(b)), the balance of the electric field will

break between polymer materials and conductive fabrics. Under electrostatic induction, the free electrons will gradually flow back to the conductive fabrics from polymer materials through the external circuits. With the external force keeping in pressing the FR-TENG, the latest achieved balance of electrostatic charge distribution will continue in being changed, which promotes the reverse flow of electrons and generates an instantaneous voltage. Once the FR-TENG is fully pressed, the negative triboelectric charges on the surface of polymer materials are completely balanced by the positive electrostatic charges induced on the conductive fabrics. If the external force is removed, the FR-TENG will bounce up to its original shapes owing to its fabric-rebound structure, while the accumulated electrons will flow back to the conductive fabrics to compensate for potential differences. After the FR-TENG returns to its released state, the positive charges on the surface of conductive fabrics will be completely neutralized by the free electrons from electrodes of polymer materials through the external circuit. Conclusively, the contact-separation processes of FR-TENG can generate an alternating electricity through an external circuit, which makes the mechanical energy from external force successfully be converted into electric energy by the FR-TENG. In the theoretical model [42-45], the potential distribution of the FR-TENG base loop under contact-separation processes (Fig. 1(e)) is quantitatively analyzed by the finite element simulation of COMSOL Multiphysics (Supplementary Fig. S2).

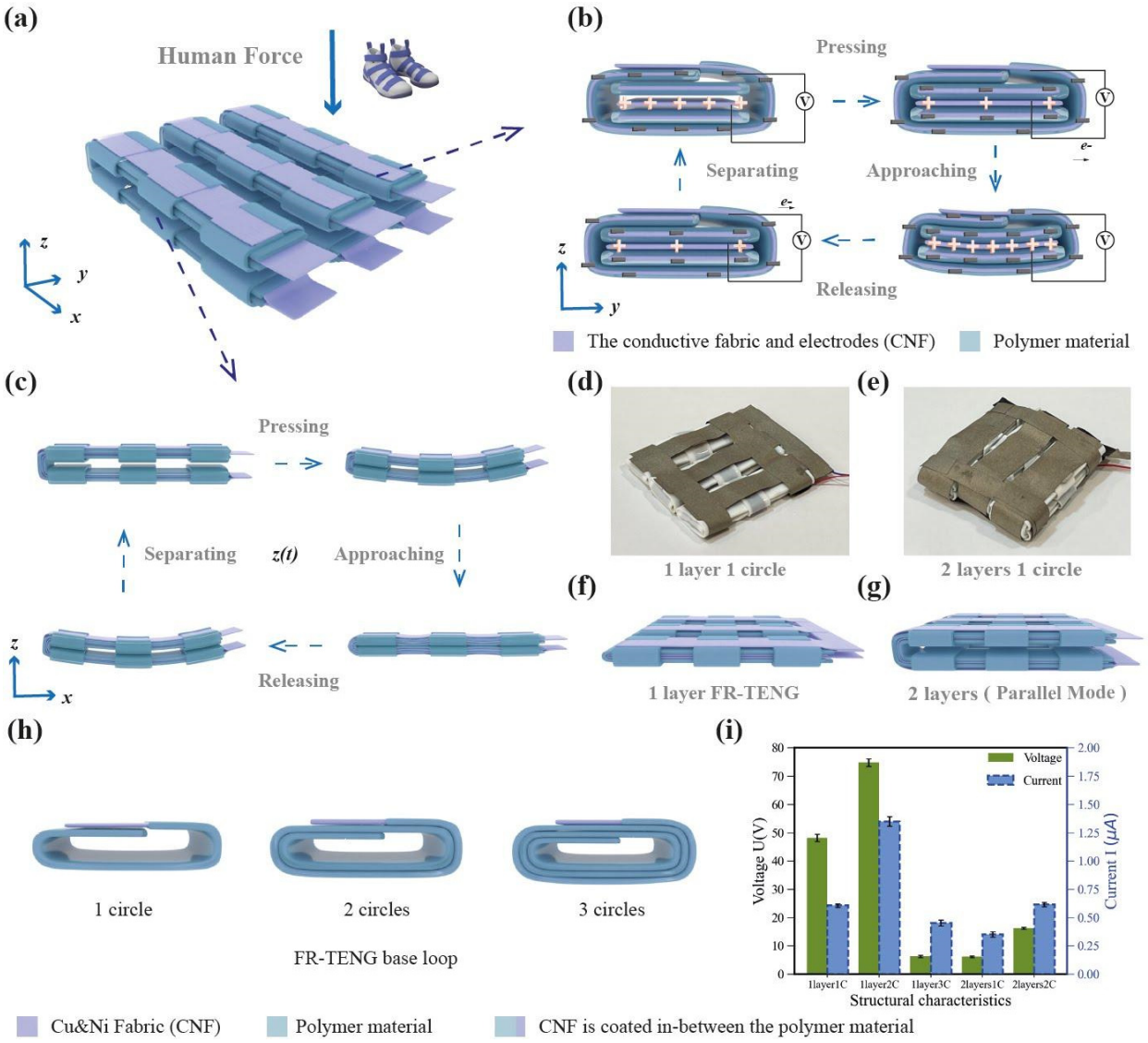

Fig. 2 Operational mechanism and structural characteristics with the performance analysis of the FR-TENGs. (a) The schematic diagram of FR-TENG, which can be impacted by the human mechanical force; (b) The accumulating processes and the transferring direction of charges in a single FR-TENG base loop; (c) The contact-separation processes between the FR-TENG base layer; (d) Optical image of FR-TENG in 1 layer 1 circle; (e) Optical image of FR-TENG in 2 layers 1 circle; (f) The demonstration of FR-TENG in 1 layer; (g) The demonstration of FR-TENG in 2 layers; (h) The samples of FR-TENG base loops in 1 circle, 2 circles and 3 circles; (i) The output voltages and currents of FR-TENGs in their different structural characteristics (C: circles, e.g. 1C means 1 circle).

Structural characteristics and optimization. Based on the circles of the FR-TENG base loop and numbers of the FR-TENG base layer in Fig. 2 and Supplementary Fig. 1, the effects of structural parameters on electric performance have been investigated in Fig. 2(i) under the impact

load of 50 N and frequency of 3 Hz. It is found that the coordination of increasing the circles and layers can be achieved in enhancing the electrical outputs. The results show that the FR-TENGs in 1 layer 2 circles (74.77 V, 1.35 μA) and 2 layers 2 circles (16.30 V, 0.62 μA) have reached better electrical outputs as compared to other numbers of structural characteristics. Although the FR-TENG in 1 layer 2 circles seems to have higher outputs than the FR-TENG in 2 layers 2 circles (parallel mode), the FR-TENG in 2 layers 2 circles was chosen for further investigation owing to its three-dimension spaces for structural optimizations. The optimizations of FR-TENGs' structures with 2 layers and 2 circles have been shown in Fig. 3, which are designed not only to keep their properties of flexibility, adaptability and rebound ability but also to enhance their electric performances. By comparing their electrical outputs in Fig. 3(i), the FR-TENG in the interval-conductive-layer model has superior performance (270.77 V, 8.18 μA and 155.59 nC) than any other structures of FR-TENGs, under the same testing conditions of the impact load at 50 N and frequency in 3 Hz. In addition, the parallel-interval mode of the FR-TENG base (Fig. 3(b)) is composed of the 2 circles of FR-TENG base loops (Fig. 3(d)) and the 7 circles of CNF rings (Fig. 3(e)-(f)), and the CNF rings mode (Fig. 3(h)) is with the 7 circles of CNF rings (Fig. 3(e)-(f)), which all resulted in ordinary performance. The variation of loading frequencies for all those structures of FR-TENGs about their output voltages and currents are explained in Supplementary Fig. S3, Supplementary Fig. S4 and Supplementary Fig. S5. All the schematic structures and respective photographs of the FR-TENGs can be found in Supplementary Fig. S6. The relationship among the structural characteristics, structural optimizations, and the electric performance of the FR-TENGs is explained in the Supplementary Note 1.

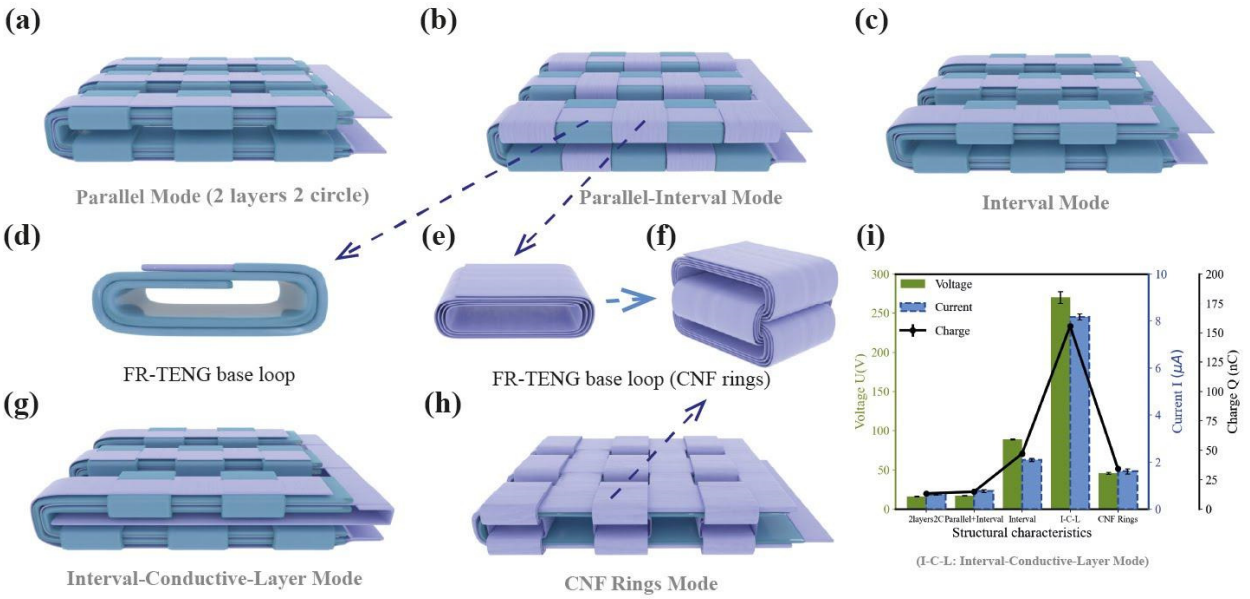

Fig. 3 Structural optimization of the FR-TENGs with their optimized structural characteristics. (a) The parallel model of FR-TENG; (b) The parallel-interval mode of FR-TENG; (c) The interval mode of FR-TENG; (d) The sample of FR-TENG base loop in its optimized characteristics which is 2 circles; (e) and (f) The sample of CNF rings in FR-TENG base loop, which was made by CNF; (g) The interval-conductive-layer mode of FR-TENG; (h) The CNF rings mode of FR-TENG; (i) Comparisons of FR-TENGs in different structures for electrical output performances, including the open-circuit voltages $U(V)$, the short-circuit currents $I(\mu A)$ and corresponding charges $Q(nC)$.

Optimized FR-TENG base and power output. As discussed above, the circuits of FR-TENG base loops and numbers of FR-TENG base layers have effects on the electrical outputs of the FR-TENGs. To quantitatively evaluate the performance of the FR-TENG base in interval-conductive-layer mode ($5 \times 5 \times 1\ cm$, length × width × height) it is necessary to study the effects of applied forces and frequencies on the FR-TENG base (Fig. 4). The frequency-dependent ($1.5\ Hz \sim 4\ Hz$) outputs of the FR-TENG base are measured under the impact force of $50\ N$ (Fig. 4(i)-(j)) by machine, including the open-circuit voltage (U) and short-circuit current (I). Since the operational mechanism of FR-TENG explained the phenomena of positive and negative electric pulses in the cyclic contact-separation processes provided by FR-TENG, the maximum outputs of FR-TENG have been evaluated by their absolute values. The results show that the output voltages are slightly changed and keep the maximum pulse at about $270\ V$ but currents are gradually increased from $7.39\ \mu A$ to $9.01\ \mu A$ with the frequencies from $1.5\ Hz$ increased to $4\ Hz$. Meanwhile, the effects of applied forces for the FR-TENG base are measured under the loading frequency of $3\ Hz$, from $20\ N \sim 50\ N$ (Fig. 4(k)-(l)) and $150\ N \sim 600\ N$ (Fig. 4(q)-(r)) by machine. It is found that with the applied forces increased the maximum pulse of voltages and currents increased from $198.41\ V$ and $6.59\ \mu A$ to $270.77\ V$ and $8.18\ \mu A$, $235.92\ V$ and $6.92\ \mu A$ to $307.15\ V$ and $10.84\ \mu A$, respectively. To balance the loading forces and frequencies between machine and human motion, frequency of $3\ Hz$ and the applied force of $50\ N$ and $600\ N$ are used for quantifying the power output of the FR-TENG base in interval-conductive-layer mode. Under the impact force of $50\ N$ and frequency of $3\ Hz$, the effective charge density (Fig. 4 (o)) reaches $5.94\ nC \cdot cm^{-2}$, and the current density and voltage density reach the same point (Fig. 4 (m)) whereas the maximum power density of $55.55\ \mu W \cdot cm^{-2}$ was achieved for an external load resistance of $\sim 30\ M\Omega$ (Fig. 4(n)). This electric energy can also be used to charging capacitors of $10\ \mu F$, $47\ \mu F$, $100\ \mu F$ and $220\ \mu F$ (Fig. 4(p)) after rectification by a single-phase rectifier ($2A/400\ V$), with the corresponding charging rates of $75.2\ mV/s$, $23.3\ mV/s$, $11.6\ mV/s$ and $4.6\ mV/s$. Besides, with the applied condition in $600\ N$ force and $3\ Hz$ frequency, the peak power density reaches up to $100.78\ \mu W \cdot cm^{-2}$ at an external load resistance of $\sim 30\ M\Omega$ (Fig. 4(t)). The durability test for the FR-TENG base is shown in Supplementary Fig. S8, which proves that its rebound stability was stable and the output performance was slightly increased after 160,000 cycles of the continuous tests.

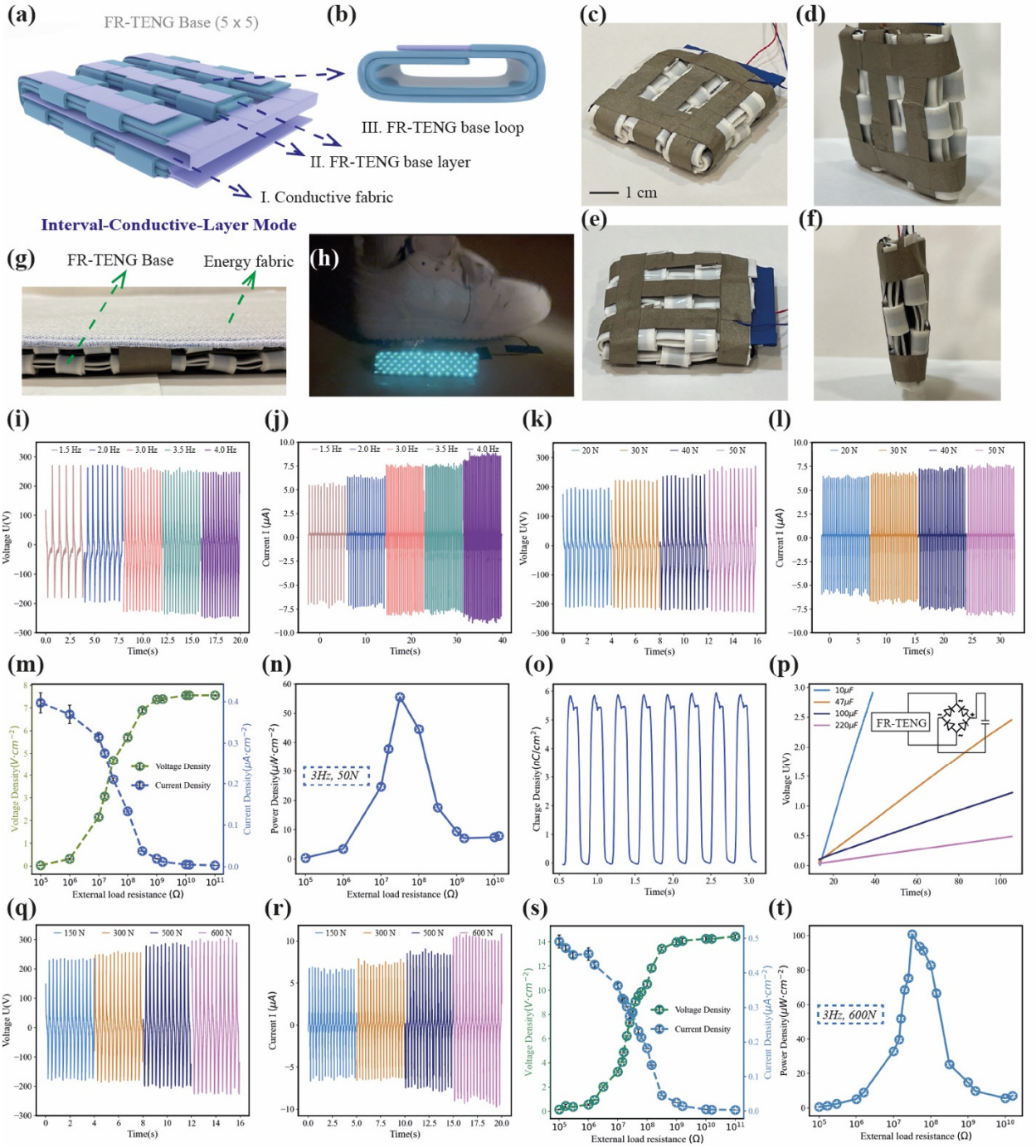

Fig. 4 The optimized structure and its electrical output performance of the FR-TENG base. (a)-(b) The schematic illustrations of the FR-TENG base in interval-conductive-layer mode, with its optical photographs (scale bar: 1 cm) in (c)-(f); (g) The photograph for FR-TENG base with energy fabric covered (Fig. 5(b)), used for (h) lighting LEDs; (i)-(j) Variations of the FR-TENG base under impact load of 50 N compared with different loading frequencies in voltage (i) and current (j); (k)-(l) Variations in voltage (k)

and current (l) of the FR-TENG base under loading frequency of 3 Hz compared with different impact forces; (m)-(p) Under the impact load of 50 N and frequency of 3 Hz, the voltage density, current density (m) and power density (n) with the load resistances from ~100 $k\Omega$ to ~10 $G\Omega$ were analyzed, while the figure of charge density (o) and the curves of charging different capacitors are presented (p) with the rectifier circuit inserted for reference; (q)-(r) Variations in voltage (q) and current (r) of the FR-TENG base under loading frequency of 3 Hz compared with different impact forces; (s)-(t) The voltage density, current density (s) and power density (t) of the FR-TENG base are further calculated by increasing the impact force to 600 N with loading frequency of 3 Hz and load resistances from ~100 $k\Omega$ to ~10 $G\Omega$.

Optimized FR-TENG module and power output. As shown in Fig. 5, the completed FR-TENG module ($5 \times 5 \times 1\ cm$, length × width × height) is composed of the FR-TENG base (Fig. 4 (a)) and energy fabric (Fig. 5(b)). Both of them (Fig. 5(c)) are studied and measured for their electric performance under 3 Hz frequency and 50 N mechanical force (277.39 V, 7.29 μA), 3 Hz frequency and 600 N mechanical force (466.61 V, 12.61 μA), as well as 1.5 Hz and 50 kg biomechanical force (418.09 V, 65.85 μA), with the corresponding maximum power density 55.94 $\mu W \cdot cm^{-2}$, 107.94 $\mu W \cdot cm^{-2}$ and 199.14 $\mu W \cdot cm^{-2}$, respectively. The generated electricity of the FR-TENG module can be used to directly light up 81 commercial LEDs (Fig. 4(h)) by simply stepping on it (Supplementary Video 1). In the meantime, those electrical energies can also be rectified and stored in capacitors (Fig. 5(q) and (r)) under the applied 3 Hz frequency and 600 N mechanical force in the mechanical testing platform, with different capacitance capacities (1 μF ~1000 μF) at the respective charging rates of 6.77 V/s, 3.95 V/s, 1.79 V/s, 0.56 V/s, 0.27 V/s and 0.033 V/s. The stored electricity in the capacitor (1000 μF) can keep the digital thermometer (TA218 with probe) working for ~60 s (Supplementary Video 2) with the charging voltage curves recorded in Fig. 5(r), which indicates the device stopped work once the stored voltage is under threshold voltage. Furthermore, the mechanical robustness, cyclic washability and working durability are also considered and investigated in this study for actual applications. It turns out the electrical output performances of the FR-TENG module are well maintained with slight fluctuation after repeatedly hand-washed for 7 times in Fig. 5(s) and continuously working for 160,000 cycles in Fig. 5(t). The observed slight fluctuation can be affected by the mechanical forces from the impact machine. The results exhibit that the FR-TENG module has excellent features in power outputs, washability, mechanical robustness, with the supports from its fabric-rebound structure. As displayed in Supplementary Table S1, the FR-TENG reveals higher electrical output performance than most previously reported TENGs [19-21, 29, 30]. Moreover, the impacts of temperature and moisture on the output performance of the FR-TENG module have also been analyzed in Supplementary Fig. S9 and Fig. S10. As the temperature rises from 4 $°C$ to 25 $°C$, the output voltage of the FR-TENG module is well maintained, and then its output performance experiences a fluctuation with the temperature further increases (Supplementary Fig. S9), which is affected by the temperature-induced changes in the ability of

electrons transferring between the conductive layer and the polymer materials. Besides, the impacts of moisture on the output performance of the FR-TENG module were also measured by spraying water droplets on the surface of the FR-TENG module. After spraying the water droplets of 0.1 g, 0.2 g, and 0.3 g, it takes 5 min, 7 min and 13 min to increase voltages that are slightly lower than the original value, respectively (Supplementary Fig. S10).

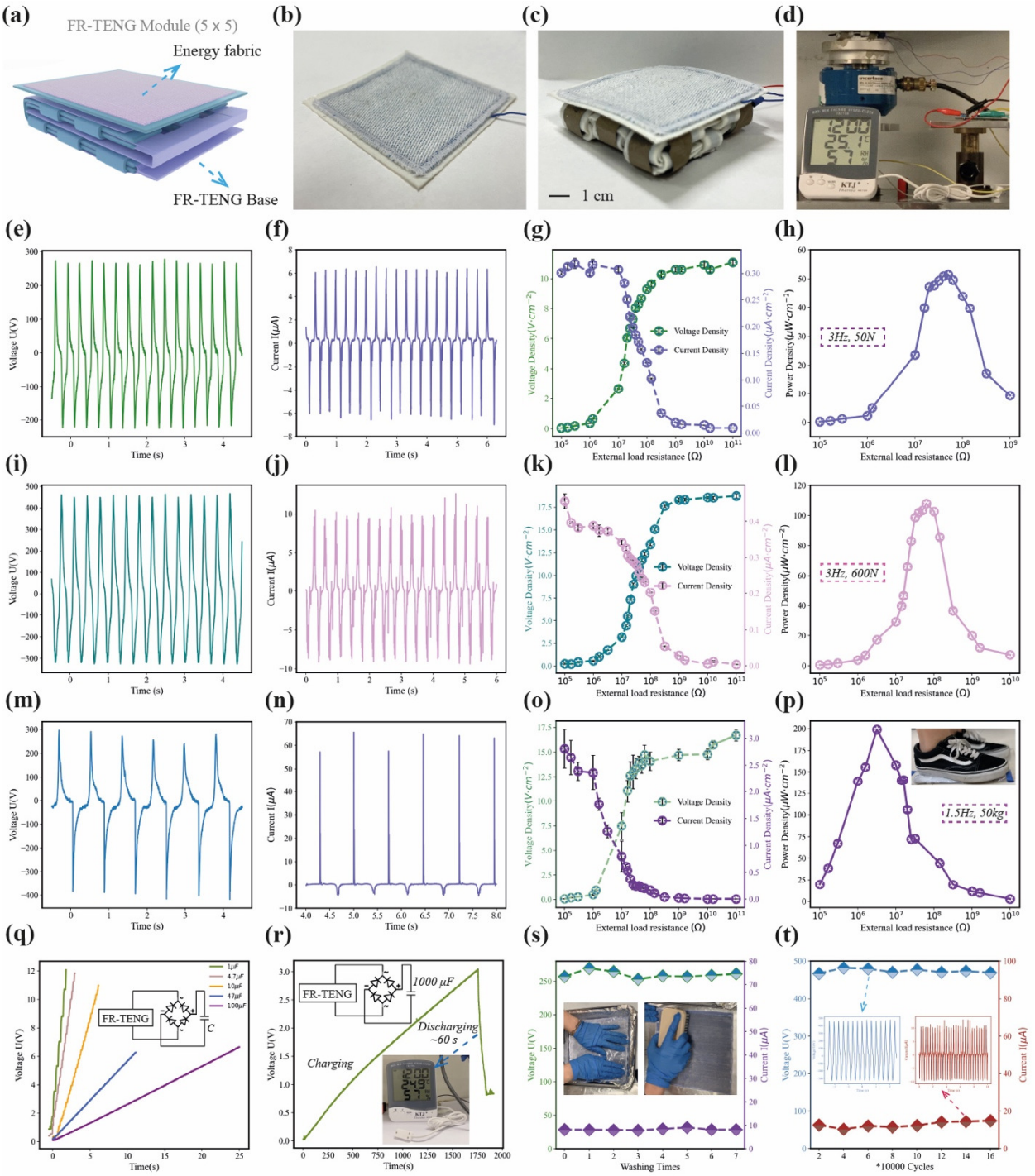

Fig. 5 The completed structure and its electrical output performance of the FR-TENG module. (a) The schematic illustrations of the FR-TENG model in interval-conductive-layer mode, with energy fabric and FR-TENG base; (b) The photograph of energy fabric; (c) The photograph of the FR-TENG module (scale bar: 1 cm); (d) The photograph of mechanical testing platform for FR-TENG to charging commercial thermometer; (e)-(h) Under the testing condition in the impact force of 50 N and the frequency of 3 Hz by machine, the output voltage (e) and current (f), as well as the voltage density, current density (g) and power density(h) of the FR-TENG module; (i)-(l) Under the testing condition in the impact force of 600 N and the frequency of 3 Hz by machine, the output voltage (i) and current (j), as well as the voltage density, current density (k) and power density (l) of the FR-TENG module; (m)-(p) Under the testing condition of the 50 kg impact and the frequency of 1.5 Hz by human, the output voltage (m) and current (n), as well as the voltage density, current density (o) and power density (p) of the FR-TENG module; (q-r) The FR-TENG module were used for charging different capacitors (1 $\mu F \sim 100\ \mu F$) in (q), and charging voltage curves of 1000 μF capacitor for powering the thermometer (r), in which the inserted photo are the related diagrams of circuits and thermometer; (s) Analysis of the cyclic washability for the FR-TENG after 7 times hand-washed at 3 Hz frequency and 50 N mechanical force. The inserted photos are the hand-washed demonstrations; (t) Analysis of the durability of the FR-TENG module by continuous test for over 160,000 cycles in 3 Hz frequency and 600 N mechanical force. The inserted photos are the voltage and current of the FR-TENG module during the durability testing.

An intelligent, wireless and self-powered carpet system. In general, using the triboelectric nanogenerator as a sustainable power source for self-powered sensing systems are commonly adopted in low energy but smart devices [46-48]. This kind of developed smart system that contains a software functional interface [8, 49] on mobile devices, can be used to record electrical signals in real-time [62]. In this paper, we developed an intelligent and self-powered carpet system in Fig. 6(a) that is based on the Bluetooth wireless technology and has the personal software application for monitoring human motion, people stream scales and fall detection with the remote emergency alarming system (Fig. 6(d)). As depicted in Fig. 6(a)-(d), the hardware module (Fig. 6(b)) for Bluetooth 4.0 (BLE 4.0) is composed of the functions of signal acquisition, wireless transmission and data processing and the software application is established in laptops for the usage of mobile phones (Fig. 6(c)). And the functional interface (Fig. 6(d)) of the software application is developed for displaying the digital voltage signals, calculating the index for people streams scales, and the customized functions for user-defined maximum values of digital voltage on the warning value of 'U', people stream scales on the warning value of 'P' and 'coefficient' of the axis. The coefficient of axis relied on the properties of the RC integrated circuit in this intelligent system (more details in Supplementary Fig. S11). As mentioned above, the alarming system depends on the threshold voltage and index from user-defined maximum values, in which the index is the summation of the digital voltage peaks. Once the maximum of the current signals is higher than the pre-defined threshold voltage 'U' or the index of the current signals is higher

than the threshold index 'P', the intelligent system will send alarming sound (Supplementary Video 5). For example, Fig. 6(e)-(h) shows the optical photographs and voltage signals of human motion from walking (Fig. 6(e)), running (Fig. 6(f)), jumping (Fig. 6(g)) and falling (Fig. 6(h)) with software interface recorded on Supplementary Video 3. The alarming for an overcrowded condition is recorded on Supplementary Video 4.

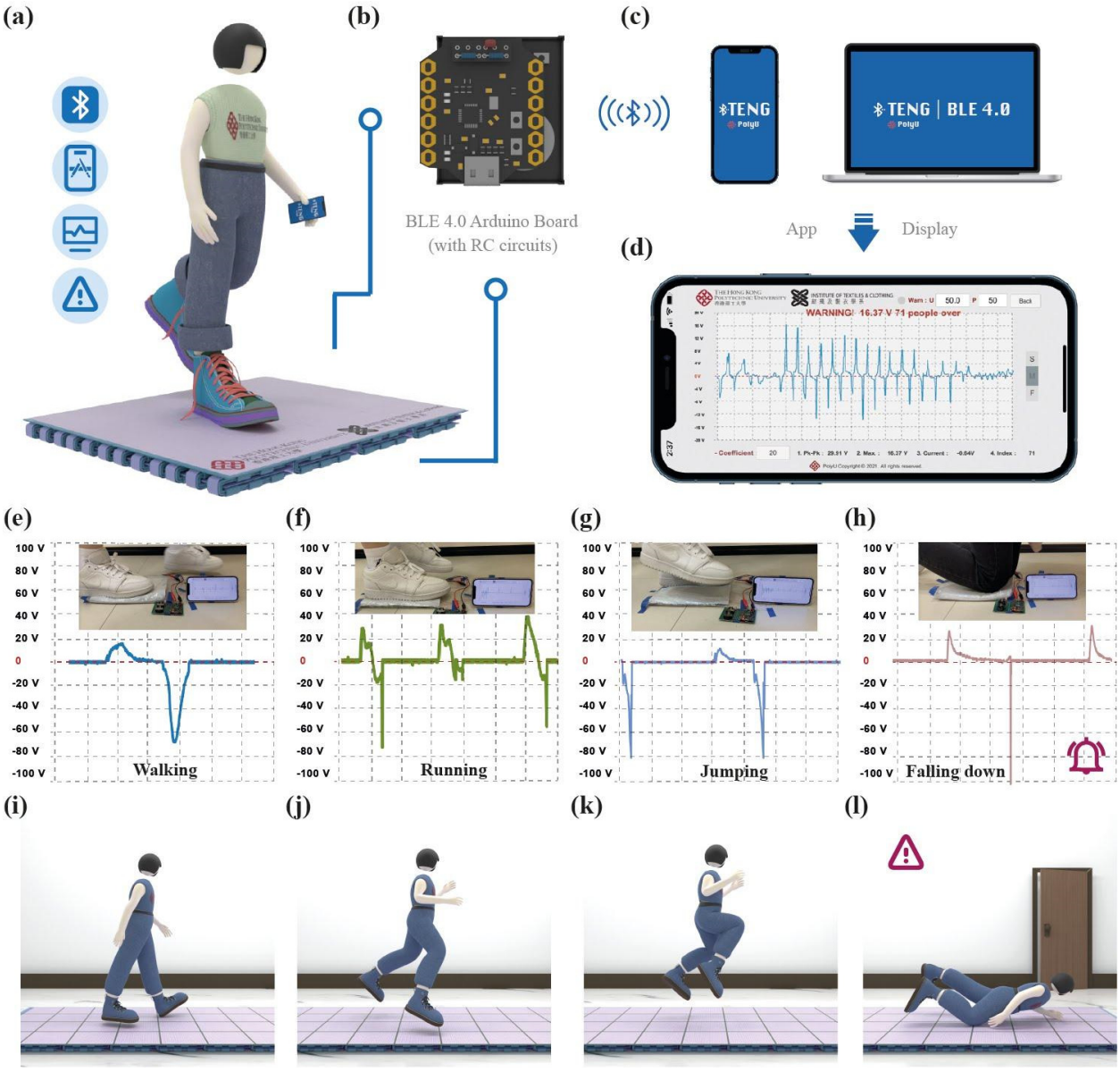

Fig. 6 An intelligent system for human motion monitoring and stream scale. (a) The schematic diagram of the intelligent system with the functions of Bluetooth mode, personal application, digital signal and alarming system; (b) The presentation of the BLE 4.0 Arduino board as the wireless transmission module for supporting the intelligent system; (c) The devices can be used for this intelligent and wireless system; (d) The software interface for the detection of digital and alarming signals, as well as the user-defined

functions; (e-h) The real-time digital voltage signals in the intelligent system for human walking (e), running (f), jumping (g) and falling (h); (i-l) The patterns of human walking (i), running (j), jumping (k) and falling (l).

3 Conclusion

In summary, we have design, developed and optimized a new kind of fabric-rebound triboelectric nanogenerator (FR-TENG) composed of loops and layered structures. With the supports of its fabric-rebound structure, the FR-TENG has been qualified with excellent features of low cost, co-friendly, high-power outputs, cyclic washability, and good mechanical robustness. In addition, the FR-TENG can be used as sustainable power sources and self-powered sensors for low-energy electronics, by converting the mechanical and biomechanical energy into electricity. Moreover, an intelligent and self-powered system with the multifunctional software application is developed and demonstrated for monitoring human motion and people stream scales, as well as remote emergency alarming for fall detection and overcrowded condition. This study provides a new structure for TENG-based e-textiles and expands its application in smart sensing carpets, which can make progress in developing self-powered sensors, human-machine interaction, and wearable technology soon.

4 Experiments

Materials. The polydimethylsiloxane (PDMS, Sylgard 184) was obtained from Dow Corning. $BaTiO_3$ nanoparticles (cubic crystalline phase, <100 nm particle size) was supplied by Aladdin, China. The conductive fabric, Cupro-Nickel fabric (CNF, CEF-1), was purchased from Suzhou Aideying Electronic Materials Co., Ltd., China. All the materials were used as received without any purification.

Fabrication processes of Energy Fabric. S twist polypropylene (PP) yarn with 60 ± 0.38 Tex linear density was spun by the ring spinning machine (Zinser 351, Saurer Schilafhorst) at 4000 rpm maximum spindle speed. Sateen fabric with cotton warp yarn and PP weft yarn is weaved by Dobby Rapier Loom Weaving Machine (SL8900, CCI Tech INC.). The fabric thickness and weight are 0.98 mm and 186.8 g/m^2 with 12 $picks/cm$ and 17 $ends/cm$ of weft and warp fabric density respectively. Prepared 9 small hook and loop fasteners (2×2 cm of each) and sewed on the surface of a CNF (20×20 cm). Stuck the CNF to the back side of the sateen fabric, overlock the edges and stuck a conductive wire on the CNF afterwards. A slide of PDMS solution film (20×20 cm) cut with 9 holes that fit with hook and loop fasteners' positions are fully covered

on the surface of CNF, adhered by the PDMS solution and placed in the oven for solidifying under 70 ℃ for 40 $mins$.

Fabrication processes of coating materials. The polydimethylsiloxane (PDMS) solution (10:1 ratio between the polymer and the cross-linker) was doped with 10% $BaTiO_3$ nanoparticles, which was coating in a mould with 0.05 cm thickness and placed in a vacuum device for removing bubbles. Then, the coated materials in the plate were placed in an oven at 80 ℃ for 1 hour until the coated materials were fully solidified. Thereafter, the conductive stripes, Cupro-Nickel fabrics (CNF) were stuck to the coated material and were covered with doped PDMS (10% $BaTiO_3$ nanoparticles) solution with 0.05 cm thickness again, which were set in a vacuum device for removing bubbles and an oven for solidifying the coated materials under 80 ℃ for 1 hour. Finally, the conductive fabric (CNF) was coated in-between PDMS (10% $BaTiO_3$ nanoparticles) solution.

Preparation of FR-TENG base layers. To obtain the FR-TENG base layers, the coating materials need to be fabricated first, and the fabrication process is mentioned above. For a double layer energy fabric base, as one FR-TENG is constructed by two base layers, six strips of base layers are needed. Therefore, an 11.5 $cm \times 9\ cm$ large coating material with 6 CNF strips (1 $cm \times 10\ cm$) that coated in-between is required. The coating material is cut into 6 strips with two different lengths (11.5 $cm \times 1.5\ cm$; 11 $cm \times 1.5\ cm$) because the outer strip required a longer length, while the inner strip required a shorter length.

Preparation of FR-TENG base loops. The fabrication process of FR-TENG base loops includes the development of FR-TENG base layers and ring-shaped formatting. The FR-TENG base layers development is the same as the process mentioned above, and the desired size is 7.8 $cm \times 1\ cm$. Then, rolling up the base layer to form loops after applying PDMS solution on part of the strips as the adhesive, as shown in Fig. 1(c), and fix the loops and place them in the oven for solidifying under 100 ℃ for half-hour.

Assembling of the energy fabric base. One end of the conductive fabric is adhered to one side of the base layer's strip by the PDMS solution, laid flat and placed in the oven for solidifying under 100 ℃ for 20 $mins$. Placing another base layer on top and insert three base loops with 1 cm interval, adhering the base layers and loops with PDMS solution. After solidification, bending the remaining part of the base layer to the top and inserting the loops, and repeating the process. Lastly, connect all the base loops and layers by CNF stripes, while the conductive fabric is connected by another CNF strip.

Washing procedure. The washing test procedure follows the AATCC Test Method 138-2005 standard, Cleaning: Washing of Textile Floor Covering. The test specimen is washed by hand scrubbing by using a polypropylene scrub brush and surfactant cleaning solution (0.3 ml of the 1.0% solution of sodium lauryl sulfate for every 645 mm^2 of pile surface) with tap water at 50 $°C \pm 3$ $°C$ for 7 times. The test specimen is rinsed with warm tap water at 50 $°C \pm 3$ $°C$ and dried in the oven set at 105 $°C \pm 5$ $°C$ after each washing. The test specimen has been cooled down after drying and before test work.

Characteristics and Measurements. An advanced keyboard life tester (ZX-A03) was used to provide the mechanical impacts with different forces and frequencies. The measurements of voltage were recorded by an oscilloscope (DSO-X-3014A), and the charge and current were recorded by an electrometer (Keithley 6514).

Acknowledgements

The authors would like to acknowledge the funding support from Innovation and Technology Commission of the Government of the Hong Kong Special Administrative Region (Project No. ITS/086/19) for the work reported here. The authors would also like to acknowledge Bernotech Limited, Fatshion Manufacturing Co., and High Quality Manufacturing Co. Ltd for their kind supports in the funded research project.

Reference

[1] J. Pei, L. Deng, S. Song, M. Zhao, Y. Zhang, S. Wu, G. Wang, Z. Zou, Z. Wu, W. He, F. Chen, N. Deng, S. Wu, Y. Wang, Y. Wu, Z. Yang, C. Ma, G. Li, W. Han, H. Li, H. Wu, R. Zhao, Y. Xie, L. Shi. Towards artificial general intelligence with hybrid Tianjic chip architecture. Nature 572 (2019) 106-111.

[2] M. Zhu, Z. Sun, T. Chen, C. Lee. Low cost exoskeleton manipulator using bidirectional triboelectric sensors enhanced multiple degree of freedom sensory system. Nat Commun 12 (2021) 2692.

[3] Q. Shi, Z. Zhang, T. He, Z. Sun, B. Wang, Y. Feng, X. Shan, B. Salam, C. Lee. Deep learning enabled smart mats as a scalable floor monitoring system. Nat Commun 11 (2020) 4609.

[4] W. Gao, S. Emaminejad, H.Y.Y. Nyein, S. Challa, K. Chen, A. Peck, H.M. Fahad, H. Ota, H. Shiraki, D. Kiriya, D.H. Lien, G.A. Brooks, R.W. Davis, A. Javey. Fully integrated wearable sensor arrays for multiplexed in situ perspiration analysis. Nature 529 (2016) 509-514.

[5] X. Zhang, J. Grajal, J.L. Vazquez-Roy, U. Radhakrishna, X. Wang, W. Chern, L. Zhou, Y. Lin, P.C. Shen, X. Ji, X. Ling, A. Zubair, Y. Zhang, H. Wang, M. Dubey, J. Kong, M. Dresselhaus, T. Palacios. Two-dimensional MoS2-enabled flexible rectenna for Wi-Fi-band wireless energy harvesting. Nature 566 (2019) 368-372.

[6] J. Kim, A.S. Campbell, B.E. de Avila, J. Wang. Wearable biosensors for healthcare monitoring. Nat Biotechnol 37 (2019) 389-406.

[7] D.Y. Park, D.J. Joe, D.H. Kim, H. Park, J.H. Han, C.K. Jeong, H. Park, J.G. Park, B. Joung, K.J. Lee. Self-Powered Real-Time Arterial Pulse Monitoring Using Ultrathin Epidermal Piezoelectric Sensors. Adv Mater 29 (2017).

[8] X. Liu, C. Tang, X. Du, S. Xiong, S. Xi, Y. Liu, X. Shen, Q. Zheng, Z. Wang, Y. Wu, A. Horner, J.-K. Kim. A highly sensitive graphene woven fabric strain sensor for wearable wireless musical instruments. Materials Horizons 4 (2017) 477-486.

[9] W. Wu, L. Wang, Y. Li, F. Zhang, L. Lin, S. Niu, D. Chenet, X. Zhang, Y. Hao, T.F. Heinz, J. Hone, Z.L. Wang. Piezoelectricity of single-atomic-layer MoS2 for energy conversion and piezotronics. Nature 514 (2014) 470-474.

[10] Z.L. Wang. On Maxwell's displacement current for energy and sensors: the origin of nanogenerators. Materials Today 20 (2017) 74-82.

[11] L. Liu, W. Tang, C. Deng, B. Chen, K. Han, W. Zhong, Z.L. Wang. Self-powered versatile shoes based on hybrid nanogenerators. Nano Research 11 (2018) 3972-3978.

[12] Y. Han, Y. Feng, Z. Yu, W. Lou, H. Liu. A Study on Piezoelectric Energy-Harvesting Wireless Sensor Networks Deployed in a Weak Vibration Environment. IEEE Sensors Journal 17 (2017) 6770-6777.

[13] H. Sun, N. Pan, X. Jin, K. Deng, Z. Liu, C.-T. Lin, T. Pan, Y. Chang. Active-powering pressure-sensing fabric devices. Journal of Materials Chemistry A 8 (2020) 358-368.

[14] S. Jung, S. Hong, J. Kim, S. Lee, T. Hyeon, M. Lee, D.H. Kim. Wearable Fall Detector using Integrated Sensors and Energy Devices. Sci Rep 5 (2015) 17081.

[15] A. Chandrasekhar, N.R. Alluri, V. Vivekananthan, Y. Purusothaman, S.-J. Kim. A sustainable freestanding biomechanical energy harvesting smart backpack as a portable-wearable power source. Journal of Materials Chemistry C 5 (2017) 1488-1493.

[16] S.L. Zhang, Y.-C. Lai, X. He, R. Liu, Y. Zi, Z.L. Wang. Auxetic Foam-Based Contact-Mode Triboelectric Nanogenerator with Highly Sensitive Self-Powered Strain Sensing Capabilities to Monitor Human Body Movement. Advanced Functional Materials 27 (2017).

[17] P. Vasandani, Z.-H. Mao, W. Jia, M. Sun. Relationship between triboelectric charge and contact force for two triboelectric layers. Journal of Electrostatics 90 (2017) 147-152.

[18] T.-C. Hou, Y. Yang, H. Zhang, J. Chen, L.-J. Chen, Z. Lin Wang. Triboelectric nanogenerator built inside shoe insole for harvesting walking energy. Nano Energy 2 (2013) 856-862.

[19] P. Bai, G. Zhu, Z.H. Lin, Q. Jing, J. Chen, G. Zhang, J. Ma, Z.L. Wang. Integrated multilayered triboelectric nanogenerator for harvesting biomechanical energy from human motions. ACS Nano 7 (2013) 3713-3719.

[20] S. Li, J. Wang, W. Peng, L. Lin, Y. Zi, S. Wang, G. Zhang, Z.L. Wang. Sustainable Energy Source for Wearable Electronics Based on Multilayer Elastomeric Triboelectric Nanogenerators. Advanced Energy Materials 7 (2017).

[21] B. Chen, W. Tang, T. Jiang, L. Zhu, X. Chen, C. He, L. Xu, H. Guo, P. Lin, D. Li, J. Shao, Z.L. Wang. Three-dimensional ultraflexible triboelectric nanogenerator made by 3D printing. Nano Energy 45 (2018) 380-389.

[22] Y. Chen, B. Xu, J. Gong, J. Wen, T. Hua, C.W. Kan, J. Deng. Design of High-Performance Wearable Energy and Sensor Electronics from Fiber Materials. ACS Appl Mater Interfaces 11 (2019) 2120-2129.

[23] J. Wen, B. Xu, J. Zhou, Y. Chen. Novel high-performance asymmetric supercapacitors based on nickel-cobalt composite and PPy for flexible and wearable energy storage. Journal of Power Sources 402 (2018) 91-98.

[24] J. Wen, B. Xu, J. Zhou. Towards 3D knitted-fabric derived supercapacitors with full structural and functional integrity of fiber and electroactive materials. Journal of Power Sources 473 (2020).

[25] X. Guan, B. Xu, J. Huang, T. Jing, Y. Gao. Fiber-shaped stretchable triboelectric nanogenerator with a novel synergistic structure of opposite Poisson's ratios. Chemical Engineering Journal 427 (2022).

[26] J. Gong, B. Xu, X. Guan, Y. Chen, S. Li, J. Feng. Towards truly wearable energy harvesters with full structural integrity of fiber materials. Nano Energy 58 (2019) 365-374.

[27] J. Wen, B. Xu, Y. Gao, M. Li, H. Fu. Wearable technologies enable high-performance textile supercapacitors with flexible, breathable and wearable characteristics for future energy storage. Energy Storage Materials 37 (2021) 94-122.

[28] X. Guan, B. Xu, M. Wu, T. Jing, Y. Yang, Y. Gao. Breathable, washable and wearable woven-structured triboelectric nanogenerators utilizing electrospun nanofibers for biomechanical energy harvesting and self-powered sensing. Nano Energy 80 (2021).

[29] J. Li, B. Xu. Novel highly sensitive and wearable pressure sensors from conductive three-dimensional fabric structures. Smart Materials and Structures 24 (2015).

[30] K. Dong, X. Peng, J. An, A.C. Wang, J. Luo, B. Sun, J. Wang, Z.L. Wang. Shape adaptable and highly resilient 3D braided triboelectric nanogenerators as e-textiles for power and sensing. Nat Commun 11 (2020) 2868.

[31] J. Wen, B. Xu, J. Zhou. Toward Flexible and Wearable Embroidered Supercapacitors from Cobalt Phosphides-Decorated Conductive Fibers. Nanomicro Lett 11 (2019) 89.

[32] Y. Chen, B. Xu, J. Xu, J. Wen, T. Hua, C.-W. Kan. Graphene-based in-planar supercapacitors by a novel laser-scribing, in-situ reduction and transfer-printed method on flexible substrates. Journal of Power Sources 420 (2019) 82-87.

[33] A. Yu, W. Wang, Z. Li, X. Liu, Y. Zhang, J. Zhai. Large-Scale Smart Carpet for Self-Powered Fall Detection. Advanced Materials Technologies 5 (2020).

[34] T. Jing, B. Xu, X. Guan, Y. Yang, M. Wu, C. Jiang. Liquid-Filling Polydimethylsiloxane Composites with Enhanced Triboelectric Performance for Flexible Nanogenerators. Macromolecular Materials and Engineering 305 (2020).

[35] T. Jing, B. Xu, Y. Yang, C. Jiang, M. Wu. Interfacial modification boosted permittivity and triboelectric performance of liquid doping composites for high-performance flexible triboelectric nanogenerators. Nano Energy 78 (2020).

[36] Z. Li, B. Xu, J. Han, J. Huang, K.Y. Chung. Interfacial Polarization and Dual Charge Transfer Induced High Permittivity of Carbon Dots-Based Composite as Humidity-Resistant Tribomaterial for Efficient Biomechanical Energy Harvesting. Advanced Energy Materials 11 (2021).

[37] X. Fan, N. Wang, J. Wang, B. Xu, F. Yan. Highly sensitive, durable and stretchable plastic strain sensors using sandwich structures of PEDOT:PSS and an elastomer. Materials Chemistry Frontiers 2 (2018) 355-361.

[38] J. Huang, X. Guan, B. Xu, J. Gong, Y. Gao, M. Li. Surface porous microstructured fibers with customized functionalities for 1D functional materials. Composites Part B: Engineering 223 (2021).

[39] J. Wen, B. Xu, J. Zhou, J. Xu, Y. Chen. 3D Patternable Supercapacitors from Hierarchically Architected Porous Fiber Composites for Wearable and Waterproof Energy Storage. Small 15 (2019) e1901313.

[40] C. Yao, A. Hernandez, Y. Yu, Z. Cai, X. Wang. Triboelectric nanogenerators and power-boards from cellulose nanofibrils and recycled materials. Nano Energy 30 (2016) 103-108.

[41] C. Liu, J. Li, L. Che, S. Chen, Z. Wang, X. Zhou. Toward large-scale fabrication of triboelectric nanogenerator (TENG) with silk-fibroin patches film via spray-coating process. Nano Energy 41 (2017) 359-366.

[42] L. Cheng, Q. Xu, Y. Zheng, X. Jia, Y. Qin. A self-improving triboelectric nanogenerator with improved charge density and increased charge accumulation speed. Nat Commun 9 (2018) 3773.

[43] S. Ankanahalli Shankaregowda, R.F. Sagade Muktar Ahmed, Y. Liu, C. Bananakere Nanjegowda, X. Cheng, S. Shivanna, S. Ramakrishna, Z. Yu, X. Zhang, K. Sannathammegowda. Dry-Coated Graphite onto Sandpaper for Triboelectric

Nanogenerator as an Active Power Source for Portable Electronics. Nanomaterials (Basel) 9 (2019).

[44] C. Wu, R. Liu, J. Wang, Y. Zi, L. Lin, Z.L. Wang. A spring-based resonance coupling for hugely enhancing the performance of triboelectric nanogenerators for harvesting low-frequency vibration energy. Nano Energy 32 (2017) 287-293.

[45] G.-H. Lim, S.S. Kwak, N. Kwon, T. Kim, H. Kim, S.M. Kim, S.-W. Kim, B. Lim. Fully stretchable and highly durable triboelectric nanogenerators based on gold-nanosheet electrodes for self-powered human-motion detection. Nano Energy 42 (2017) 300-306.

[46] S.-B. Jeon, Y.-H. Nho, S.-J. Park, W.-G. Kim, I.-W. Tcho, D. Kim, D.-S. Kwon, Y.-K. Choi. Self-powered fall detection system using pressure sensing triboelectric nanogenerators. Nano Energy 41 (2017) 139-147.

[47] X.X. Zhu, X.S. Meng, S.Y. Kuang, X.D. Wang, C.F. Pan, G. Zhu, Z.L. Wang. Triboelectrification-enabled touch sensing for self-powered position mapping and dynamic tracking by a flexible and area-scalable sensor array. Nano Energy 41 (2017) 387-393.

[48] X. Yu, Z. Xie, Y. Yu, J. Lee, A. Vazquez-Guardado, H. Luan, J. Ruban, X. Ning, A. Akhtar, D. Li, B. Ji, Y. Liu, R. Sun, J. Cao, Q. Huo, Y. Zhong, C. Lee, S. Kim, P. Gutruf, C. Zhang, Y. Xue, Q. Guo, A. Chempakasseril, P. Tian, W. Lu, J. Jeong, Y. Yu, J. Cornman, C. Tan, B. Kim, K. Lee, X. Feng, Y. Huang, J.A. Rogers. Skin-integrated wireless haptic interfaces for virtual and augmented reality. Nature 575 (2019) 473-479.

[49] Z. Zhang, T. He, M. Zhu, Z. Sun, Q. Shi, J. Zhu, B. Dong, M.R. Yuce, C. Lee. Deep learning-enabled triboelectric smart socks for IoT-based gait analysis and VR applications. npj Flexible Electronics 4 (2020).

[50] Y. Su, W. Li, L. Yuan, C. Chen, H. Pan, G. Xie, G. Conta, S. Ferrier, X. Zhao, G. Chen, H. Tai, Y. Jiang, J. Chen. Piezoelectric fiber composites with polydopamine interfacial layer for self-powered wearable biomonitoring. Nano Energy 89 (2021).

[51] Y. Su, C. Chen, H. Pan, Y. Yang, G. Chen, X. Zhao, W. Li, Q. Gong, G. Xie, Y. Zhou, S. Zhang, H. Tai, Y. Jiang, J. Chen. Muscle Fibers Inspired High-Performance Piezoelectric Textiles for Wearable Physiological Monitoring. Advanced Functional Materials 31 (2021).

[52] C.K. Jeong, D.Y. Hyeon, G.-T. Hwang, G.-J. Lee, M.-K. Lee, J.-J. Park, K.-I. Park. Nanowire-percolated piezoelectric copolymer-based highly transparent and flexible self-powered sensors. Journal of Materials Chemistry A 7 (2019) 25481-25489.

[53] A. Ahmed, I. Hassan, A.S. Helal, V. Sencadas, A. Radhi, C.K. Jeong, M.F. El-Kady. Triboelectric Nanogenerator versus Piezoelectric Generator at Low Frequency (<4 Hz): A Quantitative Comparison. iScience 23 (2020) 101286.

[54] Y. Su, J. Wang, B. Wang, T. Yang, B. Yang, G. Xie, Y. Zhou, S. Zhang, H. Tai, Z. Cai, G. Chen, Y. Jiang, L.Q. Chen, J. Chen. Alveolus-Inspired Active Membrane Sensors for Self-

Powered Wearable Chemical Sensing and Breath Analysis. ACS Nano 14 (2020) 6067-6075.

[55] Y. Su, T. Yang, X. Zhao, Z. Cai, G. Chen, M. Yao, K. Chen, M. Bick, J. Wang, S. Li, G. Xie, H. Tai, X. Du, Y. Jiang, J. Chen. A wireless energy transmission enabled wearable active acetone biosensor for non-invasive prediabetes diagnosis. Nano Energy 74 (2020).

[56] Y. Su, G. Xie, H. Tai, S. Li, B. Yang, S. Wang, Q. Zhang, H. Du, H. Zhang, X. Du, Y. Jiang. Self-powered room temperature NO2 detection driven by triboelectric nanogenerator under UV illumination. Nano Energy 47 (2018) 316-324.

[57] Y. Su, G. Xie, S. Wang, H. Tai, Q. Zhang, H. Du, H. Zhang, X. Du, Y. Jiang. Novel high-performance self-powered humidity detection enabled by triboelectric effect. Sensors and Actuators B: Chemical 251 (2017) 144-152.

[58] S. Zhang, S.T. Le, C.A. Richter, C.A. Hacker. Improved contacts to p-type MoS2 transistors by charge-transfer doping and contact engineering. Appl Phys Lett 115 (2019).

[59] S. Wang, Y. Jiang, H. Tai, B. Liu, Z. Duan, Z. Yuan, H. Pan, G. Xie, X. Du, Y. Su. An integrated flexible self-powered wearable respiration sensor. Nano Energy 63 (2019).

[60] J. Wang, S. Li, F. Yi, Y. Zi, J. Lin, X. Wang, Y. Xu, Z.L. Wang. Sustainably powering wearable electronics solely by biomechanical energy. Nat Commun 7 (2016) 12744.

[61] K.D. X. Peng, C. Ye, Y. Jiang, S. Zhai, R. Cheng, D. Liu, X. Gao, J. Wang, Z.L. Wang. A breathable, biodegradable, antibacterial, and self-powered electronic skin based on all-nanofiber triboelectric nanogenerators. Sci. Adv. 6 (2020) Article eaba9624.

[62] Y. Su, G. Chen, C. Chen, Q. Gong, G. Xie, M. Yao, H. Tai, Y. Jiang, J. Chen. Self-Powered Respiration Monitoring Enabled By a Triboelectric Nanogenerator. Adv Mater 33 (2021) e2101262.